Fast inelastic ion-ion, ion-electron, and ion-positron collisions

M. C. Chidichimo and D. W. Schranz
Department of Applied Mathematics, University of Waterloo, Waterloo, Ontario, Canada N2L 3G1

B. Zygelman
Department of Physics, University of Nevada-Las Vegas, Las Vegas, Nevada 89154
(Received 17 March 1993; revised manuscript received 30 June 1993)

We present scaling relations for the total cross sections and collision strengths of bound-state excitation in positive ions. The colliding particle can be positively or negatively charged and can be a fully ionized atom, an electron, or a positron. We consider collisions in which the kinetic energy of relative motion is large and consequently the adiabaticity parameter $\xi \ll 1$. We illustrate our general method by calculating collision strengths for proton-impact excitation of fine-structure transitions in hydrogenlike ions. The limiting case of infinite nuclear charge is also included in our calculations. Using a unitarized Coulomb-Born approximation, we show that, for dipole transitions, colliding particles with large orbital angular momenta ($l \gtrsim 2000$) make an important contribution ($\sim 70\%$) to the collision strength of proton-impact excitation. For a nonrelativistic projectile energy $E_i \to \infty$, we use the Born approximation to obtain the scaled collision strengths. These limiting values, dependent only on the particular transition, confirm the correct high-energy behavior of our data. We also use the interactive graphics computer program OMEUPS [Burgess and Tully, Astron. Astrophys. **254**, 436 (1992)] to extrapolate our data to higher energies.

PACS number(s): 34.10.+x, 34.50.Fa, 34.80.Kw

I. INTRODUCTION

Total cross sections for the excitation of positive ions by particles by arbitrary charge and mass are needed in the analysis of fusion and astrophysical plasmas and laboratory x-ray lasers. We have developed a scaling approach for the evaluation of these quantities. To unravel the complex dynamics of terrestial and astrophysical plasma we need information on the electron and ion densities and the electron and ion temperature distributions. Atomic data for the excitation rate of positive ions by electrons and ion impact are therefore essential to the deduction of temperatures and density parameters from the emission spectrum of a hot plasma [1,2].

Most of the previous quantal calculations on bound-state excitation in ion-ion collisions have been confined to the low-energy and intermediate-energy region of the impact energy [3–5], and work in this subject has been reviewed by Percival [6], Dalgarno [7], Reid [8], and Walling and Weisheit [9]. The semiclassical treatment has been used to treat a variety of inelastic ion-ion collisions involving very fast ions [9], although the accuracy of the semiclassical approximation may be questionable when the relative velocity is large. Our purpose is to extend to the high-energy range the calculations of ion-impact collisional transitions among fine-structure levels of hydrogenic ions.

We have used a unitarized Coulomb-Born approximation to consider all transitions among states having the $n=2$ principal quantum number of hydrogenlike ions. The limiting case of infinite nuclear charge is also included in our calculations. We show that colliding particles with large orbital angular momenta make an important contribution (60–70 %) to the total collision strength of proton-impact excitation of dipole-allowed transitions in positive ions. This work also stresses the importance and the significant effect that short-range interactions have on quadrupole transitions at high proton-impact energies. We have used atomic units throughout this paper, except for energies where we have used rydberg units.

II. THEORY

For any atomic transition from an initial state i to a final state f, induced by the time-dependent electric field generated by the incident particle, the relationship between the total cross section Q_{if} and the dimensionless collision strength Ω_{if} is $Q_{if}=\pi\Omega_{if}/\omega_i k_i^2$. This formula is valid for incident particles with arbitrary mass. If Hartree's atomic units are used, then the square wave number k_i^2 is numerically equal to the reduced mass M expressed in electron mass times the initial kinetic energy of relative motion E_i in rydbergs (13.6058 eV) and the total cross section Q_{if} is measured in πa_0^2 units ($8.797\,35\times10^{-17}$ cm^2). The cross section Q_{if} depends mainly on the velocity of the incident particle and the magnitude of its charge, irrespective of its mass; therefore we write the scaled total cross section $(Z_1+1)^4 Q_{if}$, measured in πa_0^2 units, in terms of a dimensionless scaled collision strength $\hat{\Omega}_{if}$ by the following equations:

$$(Z_1+1)^4 Q_{if}=\frac{\hat{\Omega}_{if}}{\omega_i K_i^2}(\pi a_0^2) \tag{1}$$

and

$$\hat{\Omega}_{if}=\frac{(Z_1+1)^2}{M^2 Z_2^2}\Omega_{if}\,, \tag{2}$$

where

$$K_i=\frac{v_i}{(Z_1+1)Z_2}\,. \tag{3}$$

The dimensionless parameter K_i is numerically equal to the magnitude of the scaled initial velocity of relative motion $v_i/(Z_1+1)Z_2$ measured in $e^2/\hbar$ units ($2.187\,69\times10^8$ cm s^{-1}), M is the reduced mass of the projectile and the ion in electron mass units ($M=1$ for electrons and positrons), Z_1 is the ion charge number, Z_2 is the projectile charge number ($Z_2^2=1$ for protons, electrons, and positrons), and ω_i is the degeneracy of the initial state.

Our objective is the calculation of $\hat{\Omega}_{if}$ when the initial kinetic energy of relative motion $E_i=(Z_1+1)^2 Z_2^2 M K_i^2$ (Ry) is large.

The collision strength $\hat{\Omega}_{if}$ has the partial wave expansion

$$\hat{\Omega}_{if}=\sum_{l_i=0}^{\infty}\sum_{l_f}\hat{\Omega}_{l_f l_i}\,, \tag{4}$$

where l_i and l_f are the initial and final quantum numbers of the colliding particle. The expression for $\hat{\Omega}_{l_f l_i}$ in terms of the scaled transmission matrix $\hat{\mathbf{T}}$ is

$$\hat{\Omega}_{l_f l_i}=\sum_J (2J+1)|\hat{T}(n_i L_i J_i l_i, n_f L_f J_f l_f; J)|^2\,, \tag{5}$$

where $n_i L_i J_i$ denotes the target states and J is the conserved total angular momenta. We represent the coupled states $n_i L_i J_i l_i J$ of the system by a subscript μ according to the scheme [10]

n_i	L_i	J_i	l_i	J	μ	parity
2	0	$\frac{1}{2}$	$J-\frac{1}{2}$	J	1(A)	$(-1)^{J-1/2}$
2	1	$\frac{1}{2}$	$J+\frac{1}{2}$	J	2(A)	$(-1)^{J-1/2}$
2	1	$\frac{3}{2}$	$J-\frac{3}{2}$	J	3(A)	$(-1)^{J-1/2}$
2	1	$\frac{3}{2}$	$J+\frac{1}{2}$	J	4(A)	$(-1)^{J-1/2}$
2	0	$\frac{1}{2}$	$J+\frac{1}{2}$	J	1(B)	$(-1)^{J+1/2}$
2	1	$\frac{1}{2}$	$J-\frac{1}{2}$	J	2(B)	$(-1)^{J+1/2}$
2	1	$\frac{3}{2}$	$J-\frac{1}{2}$	J	3(B)	$(-1)^{J+1/2}$
2	1	$\frac{3}{2}$	$J+\frac{3}{2}$	J	4(B)	$(-1)^{J+1/2}$

We label the states with parity $(-1)^{J-1/2}$ as A states and those with parity $(-1)^{J+1/2}$ as B states and introduce a concise notation for the matrix elements

$$\hat{T}_{\mu_i\mu_f}(J,A|B)=\hat{T}(n_i L_i J_i l_i, n_f L_f J_f l_f; J, A|B)\,. \tag{6}$$

We are interested in evaluating collision strengths for all values of the charge (Z_1+1) seen by the valence electron, including the limit $Z_1\to\infty$. Extending Burgess, Hummer, and Tully's [11] approach we scale out the main (Z_1+1) dependence as follows:

$$\mathcal{P}(nL|u)=(Z_1+1)^{-1/2}P_{nL}((Z_1+1)|r) \tag{7}$$

and

$$\beta^{-1/2}\mathcal{J}(\kappa l|\rho)=\beta^{-1/2}(Z_1 Z_2 M)^{1/2}F_{kl}(Z_1|R)\,, \tag{8}$$

where

$$\beta=\frac{Z_1}{Z_1+1},\quad \kappa=\frac{k}{MZ_1Z_2}=\beta^{-1}K\,,$$
$$u=(Z_1+1)r,\quad \rho=MZ_1Z_2R\,. \tag{9}$$

Then

$$\int \mathcal{P}(n_i L_i|u)\mathcal{P}(n_f L_i|u)du=\delta_{n_i n_f} \tag{10}$$

and

$$\beta^{-1/2}\mathcal{J}(\kappa l|\rho)$$
$$=\beta^{-1/2}\frac{|\Gamma(l+1+i/\kappa)|}{2\kappa^{1/2}(2l+1)!}e^{-2\pi/\kappa}(2\kappa\rho)^{l+1}e^{i\kappa\rho}$$
$$\times{}_1F_1\left[l+1+\frac{i}{\kappa},2l+2;-2i\kappa\rho\right]\,, \tag{11}$$

while asymptotically [12]

$$\beta^{-1/2}\mathcal{J}(\kappa l|\rho)$$
$$\sim\beta^{-1/2}\kappa^{-1/2}\sin\left[\kappa\rho-\frac{\ln(2\kappa\rho)}{\kappa}-\frac{\pi l}{2}+\arg\Gamma\left[l+1+\frac{i}{\kappa}\right]\right]\,. \tag{12}$$

The scaled transmission matrix $\hat{\mathbf{T}}$ in terms of the scaled reactance matrix $\hat{\mathbf{R}}$ is given by

$$\hat{\mathbf{T}}^{\mathrm{CBII}}=\frac{-2i\hat{\mathbf{R}}^{\mathrm{CB}}}{\mathbf{1}-i\left[\frac{(Z_1+1)}{MZ_2}\right]^{-1}\hat{\mathbf{R}}^{\mathrm{CB}}}\,. \tag{13}$$

We refer to this unitarization scheme as approximation II (strong coupling). If $\hat{R}^{\mathrm{CB}}_{\mu_i\mu_f}\ll1$, the $\hat{\mathbf{T}}^{\mathrm{CB}}$ matrix can be written as

$$\hat{\mathbf{T}}^{\mathrm{CBI}}=-2i\hat{\mathbf{R}}^{\mathrm{CB}}\,, \tag{14}$$

which is referred to as approximation I (weak coupling). In the limiting case $Z_1=\infty$ approximations I and II become identical.

We formulate the theory for an ion with one electron outside a closed shell and separate the $\hat{R}^{\mathrm{CB}}_{\mu_i\mu_f}$ matrix elements into two components

$$\hat{\mathbf{R}}^{\mathrm{CB}}=\hat{\mathbf{R}}^{\mathrm{SR}}+\hat{\mathbf{R}}^{\mathrm{CBe}}\,, \tag{15}$$

the short-range contribution $\hat{\mathbf{R}}^{\mathrm{SR}}$ and the long-range contribution $\hat{\mathbf{R}}^{\mathrm{CBe}}$ (Coulomb-Bethe approximation). The short-range component is defined by

$$\hat{R}^{\mathrm{SR}}_{\mu_i\mu_f}=2\left\{-\delta_{\mu_i\mu_f}b^{-1}\int_0^\infty \mathcal{F}(\kappa_i l_i|\rho)\left[\frac{Z_{\mathrm{eff}}(\rho)}{(Z_1+1)}\right]\rho^{-1}\mathcal{F}(\kappa_f l_f|\rho)d\rho\right.$$
$$+\delta_{l_i l_f}\delta_{J_i J_f}b^{-2}\int_0^\infty \mathcal{F}(\kappa_i l_i|\rho)\mathcal{F}(\kappa_f l_f|\rho)s_0\left[n_iL_i,n_fL_f;\frac{\rho}{b}\right]d\rho$$
$$\left.+b^{-2}\sum_{\lambda\,(\geq 1)}\Lambda^{l_iJ_iL_i}_{l_fJ_fL_f}(\lambda,J)\int_0^\infty \mathcal{F}(\kappa_i l_i|\rho)\mathcal{F}(\kappa_f l_f|\rho)s_\lambda\left[n_iL_i,n_fL_f;\frac{\rho}{b}\right]d\rho\right\}. \tag{16}$$

The function $Z_{\mathrm{eff}}(\rho)$, defined by $Z_0+Z_{\mathrm{eff}}(\rho)-N=Z(\rho)$ with $Z_{\mathrm{eff}}(\infty)=0$ and $Z_{\mathrm{eff}}(0)=N-1$, measures the increase in the effective nuclear charge number $Z_0+Z_{\mathrm{eff}}(\rho)$ as the incident particle penetrates the electron cloud. Z_0 is the nuclear charge number, N is the number of electrons in the ion, and $Z_1=Z_0-N$. The function $Z_{\mathrm{eff}}(\rho)$ equals 0 for all ρ in the case of hydrogenic ions.

The integral s_λ behaves as a decreasing exponential for large ρ (short-range potential) [11] and is given by

$$s_\lambda\left[n_iL_i,n_fL_f;\frac{\rho}{b}\right]$$
$$=\left[\frac{\rho}{b}\right]^\lambda\int_{\rho/b}^\infty\frac{\mathcal{P}(n_iL_i|u)\mathcal{P}(n_fL_f|u)}{u^{\lambda+1}}du$$
$$-\left[\frac{\rho}{b}\right]^{-(\lambda+1)}\int_{\rho/b}^\infty\mathcal{P}(n_iL_i|u)\mathcal{P}(n_fL_f|u)u^\lambda du\ , \tag{17}$$

where $b=MZ_2\beta$.

The CBe reactance matrix may be expressed as

$$\hat{R}^{\mathrm{CBe}}_{\mu_i\mu_f}=2b^{\lambda-1}\sum_{\lambda\,(\geq 1)}\Lambda^{l_iJ_iL_i}_{l_fJ_fL_f}(\lambda,J)B(n_iL_i,n_fL_f;\lambda)$$
$$\times I(\kappa_i l_i,\kappa_f l_f;\lambda)\ , \tag{18}$$

where the integral B is defined by

$$B(n_iL_i,n_fL_f;\lambda)=\int_0^\infty\mathcal{P}(n_iL_i|u)\mathcal{P}(n_fL_f|u)u^\lambda du \tag{19}$$

and

$$I(\kappa_i l_i,\kappa_f l_f;\lambda)=\int_0^\infty\frac{\mathcal{F}(\kappa_i l_i|\rho)\mathcal{F}(\kappa_f l_f|\rho)}{\rho^{\lambda+1}}d\rho \tag{20}$$

is an integral that may be evaluated in terms of generalized hypergeometric functions [11,13]. Λ is the angular factor [10] corresponding to fine-structure transitions and is given by

$$\Lambda^{l_iJ_iL_i}_{l_fJ_fL_f}(\lambda,J)=(-1)^{J-1/2+\lambda}\begin{Bmatrix}l_f & J_f & J\\ J_i & l_i & \lambda\end{Bmatrix}$$
$$\times\begin{bmatrix}J_i & \lambda & J_f\\ \frac{1}{2} & 0 & -\frac{1}{2}\end{bmatrix}\begin{bmatrix}l_i & \lambda & l_f\\ 0 & 0 & 0\end{bmatrix}$$
$$\times[J_i,J_f]^{1/2}[l_i,l_f]^{1/2}\ . \tag{21}$$

It is convenient to define all the collision parameters involved in our algebraic expressions as function of the initial kinetic energy E_i and the excitation energy E_{if}. The dimensionless adiabaticity parameter ξ, which is proportional to the ratio between the collision time $t=a/v_i$, where $a=Z_1Z_2e^2/Mv_iv_f$ is half the symmetrized distance of closest approach in a head-on collision [13], and the atomic period $\tau=\hbar/E_{if}$, is defined by

$$\xi=\eta_f-\eta_i=\eta_i[(1-x)^{-1/2}-1]\ , \tag{22}$$

where the dimensionless parameter η_i (ratio between $Z_1Z_2e^2/Mv_i^2$ and the wavelength $\lambda/2\pi=k_i^{-1}$ of the projectile) is given by

$$\eta_i=\frac{1}{\kappa_i}=\frac{Z_1}{K_i(Z_1+1)}=Z_1Z_2/v_i=\left[\frac{M}{E_i}\right]^{1/2}Z_1Z_2\ , \tag{23}$$

and measures the effective strength of the interaction. The parameter x is the ratio between the excitation energy E_{if} and the initial kinetic energy E_i and is given by

$$x=\frac{E_{if}}{E_i}=\frac{E_{if}}{M(Z_1+1)^2Z_2^2K_i^2}\ . \tag{24}$$

In Eqs. (22)–(24) the magnitude v_i of the velocity is measured in $e^2/\hbar$ units ($2.187\,69\times10^8$ cm s^{-1}), the reduced mass M is measured in electron masses, and E_i and E_{if} are measured in rydbergs (13.6058 eV). In the case of collisions with fast particles, the values of ξ, $x=E_{if}/E_i$, and therefore ξ/η_i are small compared with unity. For values of l such that $l\ll E_i/E_{if}$ (i.e., $l\xi/\eta_i\ll1$) the Coulomb integrals $I(\kappa_i l_i,\kappa_f l_f;\lambda)$ are independent of E_{if} and may be calculated with $E_{if}=0$ (i.e., $\xi=0$) [11]. In the limit $\xi\to0$, $\kappa_i,\kappa_f\to\kappa$ and the integrals I simplify appreciably [11,13]. For the dipole case we have

$$I(\kappa l,\kappa l+1;1)=\tfrac{1}{2}\kappa[1+(l+1)^2\kappa^2]^{-1/2} \tag{25}$$

and for the quadrupole case

$$I(\kappa l,\kappa l;2)=\frac{\pi(e^{2\pi/\kappa}-1)+\kappa^3\sum_{s=0}^{l}\frac{s^2}{(1+s^2\kappa^2)}}{l(l+1)(2l+1)} \tag{26}$$

and

$$I(\kappa l-1,\kappa l+1;2)$$
$$=\frac{\kappa^3}{6}[1+l^2\kappa^2]^{-1/2}[1+(l+1)^2\kappa^2]^{-1/2}\ . \tag{27}$$

If $\xi l/\eta_i>1$, e.g., at lower collision energies and/or larger transition energy E_{if}, Eqs. (25)–(27) are not valid.

To carry out our calculations we split Eq. (4) into two parts

$$\hat{\Omega}_{if}=\sum_{l_i=0}^{l_1}\sum_{l_f}\hat{\Omega}_{l_f l_i}+\sum_{l_i=l_{1+1}}^{\infty}\sum_{l_f}\hat{\Omega}_{l_f l_i}\ . \tag{28}$$

We choose the value l_1 such that $l_1 \ll E_i/E_{if}$ and for all $l_i > l_1$ (i) the interaction is weak, i.e., the scaled reactance matrix elements $\hat{R}_{\mu_i\mu_f} \ll 1$ and therefore $\hat{T}_{\mu_i\mu_f} \simeq -2i\hat{R}_{\mu_i\mu_f}$; and (ii) only the long-range potential $\rho^{-(\lambda+1)}$ is effective, i.e., $\hat{R}_{\mu_i\mu_f} \sim \hat{R}^{\mathrm{CBE}}_{\mu_i\mu_f}$.

III. SUM CONTRIBUTION FOR $J \le l_1+\frac{1}{2}$ AND $l_i \le l_1$

Define

$$\hat{\Omega}_J=(2J+1)\sum_{l_i l_f}|\hat{T}_{\mu_i\mu_f}(J)|^2\ . \tag{29}$$

The total scaled collision strength is then given by

$$\hat{\Omega}_{if}=\sum_{J=1/2}^{\infty}\hat{\Omega}_J\ . \tag{30}$$

We suppose that $\hat{\Omega}_J$ has been calculated for all values of J less than or equal to $J_1=l_1+\frac{1}{2}$; then for $l_i \le l_1$

$$\sum_{l_i=0}^{l_1}\sum_{l_f}\hat{\Omega}_{l_f l_i}(2p_{1/2}\text{-}2s_{1/2})=\sum_{J=1/2}^{l_1+1/2}\hat{\Omega}_J-2(l_1+1)|\hat{T}_{12}(l_1+\tfrac{1}{2},A)|^2\ , \tag{31}$$

$$\sum_{l_i=0}^{l_1}\sum_{l_f}\hat{\Omega}_{l_f l_i}(2s_{1/2}\text{-}2p_{3/2})=\sum_{J=1/2}^{l_1+1/2}\hat{\Omega}_J-2(l_1+1)[|\hat{T}_{13}(l_1+\tfrac{1}{2},B)|^2+|\hat{T}_{14}(l_1+\tfrac{1}{2},B)|^2]\ , \tag{32}$$

$$\sum_{l_i=0}^{l_1}\sum_{l_f}\hat{\Omega}_{l_f l_i}(2p_{1/2}\text{-}2p_{3/2})=\sum_{J=1/2}^{l_1+1/2}\hat{\Omega}_J-2(l_1+1)[|\hat{T}_{24}(l_1+\tfrac{1}{2},A)|^2+|\hat{T}_{23}(l_1+\tfrac{1}{2},A)|^2]\ , \tag{33}$$

where

$$\hat{\Omega}_J(2p_{1/2}\text{-}2s_{1/2})=(2J+1)[|\hat{T}_{12}(J,A)|^2+|\hat{T}_{12}(J,B)|^2]\ , \tag{34}$$

$$\hat{\Omega}_J(2s_{1/2}\text{-}2p_{3/2})=(2J+1)[|\hat{T}_{13}(J,A)|^2+|\hat{T}_{14}(J,A)|^2+|\hat{T}_{13}(J,B)|^2+|\hat{T}_{14}(J,B)|^2]\ , \tag{35}$$

and

$$\hat{\Omega}_J(2p_{1/2}\text{-}2p_{3/2})=(2J+1)[|\hat{T}_{23}(J,A)|^2+|\hat{T}_{24}(J,A)|^2+|\hat{T}_{23}(J,B)|^2+|\hat{T}_{24}(J,B)|^2]\ . \tag{36}$$

The matrix elements $\hat{T}_{\mu_i\mu_f}(J)$ have been evaluated using Eqs. (13)–(18) and (25)–(27). As J increases the short-range contribution $\hat{R}^{\mathrm{SR}}_{\mu_i\mu_f}$ becomes negligible. In practice we use the full CB approximation $\hat{R}^{\mathrm{CB}}_{\mu_i\mu_f}$ for all $J \le J_0$ and for $J_0 < J \le J_1$ we assume $\hat{R}^{\mathrm{CB}}_{\mu_i\mu_f} \sim \hat{R}^{\mathrm{CBe}}_{\mu_i\mu_f}$. We have obtained the short-range matrix elements $\hat{R}^{\mathrm{SR}}_{\mu_i\mu_f}$ by numeric integration of Eq. (16), in which the functions $\mathcal{F}(\kappa l|\rho)$ were generated by numerically integrating the Coulomb differential equation [12].

IV. SUM CONTRIBUTION FOR $l_i > l_1$

For dipole-allowed transitions the dominant part of the total collision strength $\hat{\Omega}_{if}$ comes from large angular momenta $l_i \gtrsim 2000$. On the other hand, the sum over partial wave contributions $\hat{\Omega}_{l_i l_f}$ converges rather slowly. Burgess [14,15] has discovered a sum rule for partial collision strengths, calculated in the Coulomb-Bethe approximation that overcomes this problem.

For quadrupole transitions, and $l_i \gg 1, \hat{\Omega}_{l_i}=al_i^{-3}$, where $\hat{\Omega}_{l_i}=\sum_{l_f}\hat{\Omega}_{l_f l_i}$ and $l_f=l_i, l_i\pm 2$. The high-angular-momentum contribution to $\hat{\Omega}_{if}$ is given by [16]

$$\sum_{l_i=l_1+1}^{\infty}\sum_{l_f}\hat{\Omega}_{l_f l_i}\sim\tfrac{1}{2}\hat{\Omega}_{l_1+1}+\int_{l_{1+1}}^{\infty}\hat{\Omega}_l\,dl \sim\tfrac{1}{2}\hat{\Omega}_{l_1+1}+\frac{a}{4(l_1+1)^4}\ . \tag{37}$$

The constant of proportionality a has been determined from $\hat{\Omega}_{l_1+1}$.

A. Sum rule for dipole transitions ($\lambda=1$)

Because of conditions (i) and (ii) from Sec. II we can use the CBe approximation to determine the transmission matrix elements. Thus for $J > J_1$, the scaled transmission matrix elements are given by

$$\hat{T}_{\mu_i\mu_f}=-4i\Lambda^{l_i J_i L_i}_{l_f J_f L_f}(1,J)B(n_iL_i,n_fL_f;1)I(\kappa_i l_i,\kappa_f l_f;1)\ , \tag{38}$$

where $B(2s,2p)=-3\sqrt{3}$.

The scaled partial collision strength $\hat{\Omega}_{l_f l_i}$ reduces to

$$\hat{\Omega}_{l_f l_i}=432|I(\kappa_i l_i,\kappa_f l_f;1)|^2\sum_J(2J+1)|\Lambda^{l_i J_i L_i}_{l_f J_f L_f}(1,J)|^2\ . \tag{39}$$

Using the orthogonality relations of the $6j$ symbols [17] the summation in (39) gives us

$$\sum_J(2J+1)|\Lambda^{l_i J_i L_i}_{l_f j_f L_f}(1,J)|^2=\frac{l_>(2J_>+1)}{9}\ , \tag{40}$$

where $l_>=\max(l_i,l_f)$ and $J_>=\max(J_i,J_f)$.

We use Eqs. (39) and (40) to express the high-angular-momentum contribution to the total collision strength $\hat{\Omega}_{if}$ for both dipole transitions, as

$$\sum_{l_i=l_1+1}^{\infty}\sum_{l_f}\hat{\Omega}_{l_f l_i}=48(2J_>+1)\times\sum_{l_i=l_1+1}^{\infty}\sum_{l_f}l_>|I(\kappa_i l_i,\kappa_f l_f;1)|^2 . \quad (41)$$

Using Burgess's sum rule [14],

$$\sum_{l_i=l_1+1}^{\infty}\sum_{l_f}l_>|I(\kappa_i l_i,\kappa_f l_f;1)|^2 =[I^2(\kappa_i l_1+1,\kappa_f l_1;1)-I^2(\kappa_i l_1,\kappa_f l_1+1;1)]\times\frac{(1+(l_1+1)^2\kappa_i^2)}{(l_1+1)(\kappa_i^2-\kappa_f^2)} , \quad (42)$$

we have

$$\sum_{l_i=l_1+1}^{\infty}\sum_{l_f}\hat{\Omega}_{l_f l_i}=48(2J_>+1)(l_1+1)^{-1}\times[I^2(\kappa_i l_1+1,\kappa_f l_1;1)-I^2(\kappa_i l_1,\kappa_f l_1+1;1)]\times\frac{\eta_f^2}{\xi(\eta_i+\eta_f)}[\eta_i^2+(l_1+1)^2] . \quad (43)$$

The Coulomb integral $I(\kappa_1 l,\kappa_2 l+1;1)$ is given by

$$I(\kappa_1 l,\kappa_2 l+1;1)=e^{-\pi|\xi|}I^{\rm elec}(\kappa_1 l,\kappa_2 l+1;1) , \quad (44)$$

where $\xi=\eta_2-\eta_1$ and $\eta=1/\kappa$ and $I^{\rm elec}(\kappa_1 l,\kappa_2 l+1;1)$ is the radial integral for electron impact [11];

$$I^{\rm elec}(\kappa_1 l,\kappa_2 l+1;1)=\left[\frac{2\pi|\xi|}{1-e^{-2\pi|\xi|}}\right]^{1/2}\frac{(\eta_1\eta_2)^{1/2}}{2}\left[\frac{4\eta_1\eta_2}{(\eta_1+\eta_2)^2}\right]^{l+1}\times{\rm Im}\left\{e^{i\{P_{l+1}\mp\arctan[\eta_1/(l+1)]\}}\left[\frac{\eta_1+\eta_2}{|\xi|}\right]^{i|\xi|}W\right\} , \quad (45)$$

where

$$W=\mp1+\sum_{m=1}^{\infty}\frac{\left[\prod_{p=2}^{m}(l+p\mp i\eta_2)\right]\left[\prod_{p=1}^{m}(l+p\pm i\eta_1)\right]}{\left[\prod_{p=1}^{m}(p-i|\xi|)\right]m!}\times\frac{|\xi|^{2m-1}}{(\eta_1+\eta_2)^{2m}}[-(l+1)\xi\pm i\eta_2\xi-2m\eta_2] \quad (46)$$

with $\prod_{p=2}^{1}(\cdots)$ to be taken to be 1 and

$$P_l=\arg\left[\frac{\Gamma(1+i|\xi|)}{\Gamma(l+1\mp i\eta_1)\Gamma(l+1\pm i\eta_2)}\right] . \quad (47)$$

The top sign corresponds to $\kappa_1>\kappa_2$ and the bottom sign to $\kappa_1<\kappa_2$.

For the range of the parameter K_i that we are considering we have $\xi\ll1(\eta_i,\eta_f\to\eta)$. We have been careful to remove large masking quantities when the crucial information is carried by small numbers. If $\xi\ll1$ and $\xi l_1/\eta_i\ll1$ there is cancellation between $I^2(\kappa_i l_1+1,\kappa_f l_1;1)$ and $I^2(\kappa_i l_1,\kappa_f l_1+1;1)$, which removes the effect of the ξ term in the denominator of Eq. (43). We substitute Eqs. (44) and (45) into Eq. (43) and for $l_1\ll E_i/E_{if}$ (i.e., $l_1\xi/\eta_i\ll1$ and therefore $\xi/\eta_i\ll1$); we get

$$\sum_{l_i=l_1+1}^{\infty}\sum_{l_f}\hat{\Omega}_{l_f l_i}\simeq24(2J_>+1)\left\{\ln\left[\frac{2\eta}{\xi}\right]-\sum_{s=l_1+1}^{\infty}\frac{\eta^2}{s[\eta^2+s^2]}-\frac{(l_1+1)}{2[\eta^2+(l_1+1)^2]}-\sum_{s=1}^{l_1}s^{-1}\right\} , \quad \xi\ll1,\ \frac{\xi l_1}{\eta}\ll1 . \quad (48)$$

This equation is valid for colliding particles of arbitrary charge and mass.

For any monotonically decreasing function $f(s)$ we may approximate the sum $\sum_{s=l_1+1}^{\infty}f(s)$ by [16]

$$\sum_{s=l_1+1}^{\infty}f(s)=\tfrac{1}{2}f(l_1+1)+\int_{l_1+1}^{\infty}f(s)ds ; \quad (49)$$

therefore

$$\sum_{s=l_1+1}^{\infty}\frac{\eta^2}{s(\eta^2+s^2)}\simeq\frac{1}{2}\frac{\eta^2}{(l_1+1)[\eta^2+(l_1+1)^2]}+\frac{1}{2}\ln\left[1+\frac{\eta^2}{(l_1+1)^2}\right] . \quad (50)$$

The high-angular-momentum contribution is then given by

$$\sum_{l_i=l_1+1}^{\infty}\sum_{l_f}\hat{\Omega}_{l_f l_i}\simeq 24(2J_>+1)\left\{\ln\left[\frac{2\eta}{\xi}\right]-\frac{1}{2(l_1+1)}-\sum_{s=1}^{l_1}s^{-1}-\frac{1}{2}\ln\left[1+\frac{\eta^2}{(l_1+1)^2}\right]\right\},\quad \xi\ll 1,\quad \frac{\xi l_1}{\eta}\ll 1\ . \tag{51}$$

If $l_1\gg\eta$ then

$$\sum_{l_i=l_1+1}^{\infty}\sum_{l_f}\hat{\Omega}_{l_f l_i}\simeq 24(2J_>+1)\left\{\ln\left[\frac{2\eta}{\xi}\right]-\frac{1}{2(l_1+1)}-\sum_{s=1}^{l_1}s^{-1}-\frac{1}{2}\frac{\eta^2}{(l_1+1)^2}\right\},\quad \xi\ll 1,\frac{\xi l_1}{\eta}\ll 1,\quad \frac{\eta}{l_1}\ll 1\ . \tag{52}$$

Notice that Eq. (48) may be rewritten using [18]

$$\mathrm{Re}\psi(i\eta)=\psi(1)+\eta^2\sum_{s=1}^{\infty}\frac{1}{s(s^2+\eta^2)}\ , \tag{53}$$

where ψ is the logarithmic derivative of the Γ function. Expression (48) is then reduced to

$$\sum_{l_i=l_1+1}^{\infty}\sum_{l_f}\hat{\Omega}_{l_f l_i}\simeq 24(2J_>+1)\left\{\ln\left[\frac{2\eta}{\xi}\right]+\psi(1)-\mathrm{Re}\psi(i\eta)-\sum_{l=0}^{l_1}\frac{(l+1)}{[\eta^2+(l+1)^2]}+\frac{(l_1+1)}{2[\eta^2+(l_1+1)^2]}\right\}. \tag{54}$$

Using $I(\kappa l,\kappa l+1;1)=\frac{1}{2}\kappa[1+(l+1)^2\kappa^2]^{-1/2}$ we also have

$$\sum_{l_i=l_1+1}^{\infty}\sum_{l_f}\hat{\Omega}_{l_f l_i}\simeq 48(2J_>+1)\left\{\frac{\pi}{2\sqrt{3}}g(\eta_i,\eta_f)-2\sum_{l=0}^{l_1}(l+1)I^2(\kappa l,\kappa l+1;1)+(l_1+1)I^2(\kappa l_1,\kappa l_1+1;1)\right\},$$

$$\xi\ll 1,\quad \frac{\xi l_1}{\eta}\ll 1\ , \tag{55}$$

where

$$g(\eta_i,\eta_f)\simeq\frac{\sqrt{3}}{\pi}\left[\ln\left[\frac{2\eta}{\xi}\right]+\psi(1)-\mathrm{Re}\psi(i\eta)\right],\qquad \xi\ll 1 \tag{56}$$

is the free-free Gaunt factor [13,14,19].

For $\eta\ll 1$, $\mathrm{Re}\psi(i\eta)$ has the series expansion [18]

$$\mathrm{Re}\psi(i\eta)\approx\psi(1)+1-\frac{1}{1+\eta^2}+[\zeta(3)-1]\eta^2-[\zeta(5)-1]\eta^4+\cdots,\quad \eta\ll 1 \tag{57}$$

and for $\eta\gg 1$, it has the asymptotic formula

$$\mathrm{Re}\psi(i\eta)\approx\ln\eta+\frac{1}{12\eta^2}+\frac{1}{120\eta^4}+\cdots,\quad \eta\gg 1 \tag{58}$$

where $\zeta(2n+1)$, $n=1,2,\ldots$ is the Riemann zeta function.

We should stress that, in the case of electron impact excitation, Burgess, Hummer, and Tully [11] used Eq. (55) to evaluate the high-angular-momentum contribution to $\hat{\Omega}_{if}$ with

$$g(\eta_i,\eta_f)\simeq\frac{\sqrt{3}}{\pi}\ln\left[\frac{2\eta}{\xi}\right],\quad \xi\ll 1,\ \eta\ll 1\ , \tag{59}$$

i.e., for projectiles with large $K=v/(Z_1+1)Z_2$. If $\eta\ll 1$ then $\mathrm{Re}\psi(i\eta)-\psi(1)\simeq\zeta(3)\eta^2$ [$\zeta(3)=1.202\,05\ldots$] and Eqs. (56) and (59) are equivalent to first order in η^2.

B. Geometric-series method

For the sake of completeness we should like to review the geometric-series method and two approximations associated with it. The geometric-series method has the disadvantage of only starting to become useful for $l_1\gg E_i/E_{if}$ (i.e., $l_1\xi/\eta_i\gg 1$), which makes the method impractical at the high energies considered here.

1. Born approximation

For $l_i,l_f\gg 1$, and $l_i\gg\eta_i$ we have [13]

$$I(\kappa_i l_i,\kappa_f l_f;1)\sim e^{-(\pi/2)|\xi|}I_0(\kappa_i l_i,\kappa_f l_f;\lambda)\ , \tag{60}$$

where I_0 is the radial integral for the neutral case $Z_1=0$, in which the functions $\mathcal{F}(\kappa l|\rho)$ are expressed in terms of spherical Bessel functions. The integral I_0 is given by [11]

$$I_0(\kappa_1 l,\kappa_2 l+1;1)=\frac{\pi}{4}(\kappa_1\kappa_2)^{1/2}\kappa_>^{-1}\left[\frac{\kappa_<}{\kappa_>}\right]^{l+p}\frac{\Gamma(l+1)}{\Gamma(l+\frac{3}{2}+p)\Gamma(\frac{3}{2}-p)}\times F\left[l+1,p-\frac{1}{2};l+\frac{3}{2}+p;\frac{\kappa_<^2}{\kappa_>^2}\right], \tag{61}$$

where

$$p=\begin{cases}0 & \text{if } \kappa_1<\kappa_2\\ 1 & \text{if } \kappa_1>\kappa_2\ ,\end{cases}$$

and $\kappa_>=\max(\kappa_1,\kappa_2)$ and $\kappa_<=\min(\kappa_1,\kappa_2)$.

Using [18]

$$F(a,b;c;z)=(1-z)^{-b}F\left[b,c-a;c;\frac{z}{z-1}\right] \tag{62}$$

and

$$\lim_{n\to\infty} n^{b-a}\frac{\Gamma(n+a)}{\Gamma(n+b)}=1 , \tag{63}$$

and considering the asymptotic behavior [20] of $F(b,c-a;c;z/(z-1))$ for $l\gg\kappa_<^2/(\kappa_>^2-\kappa_<^2)=E_f/E_{if}$, we have

$$I_0(\kappa_1 l,\kappa_2 l+1;1)\approx\frac{\pi^{1/2}}{2}\left[\frac{\kappa_<}{\kappa_>}\right]^{l+1/2+p}\times(l+1)^{-(p+1/2)}\left[\frac{\kappa_>^2-\kappa_<^2}{\kappa_>^2}\right]^{-p+1/2} , \qquad l\gg\frac{\kappa_<^2}{\kappa_>^2-\kappa_<^2} . \tag{64}$$

Then the contribution from $l_i=l>l_1$ [Eq. (41)] to the total collision strength $\hat{\Omega}_{if}$ is, for $l\gg\kappa_i^2/(\kappa_i^2-\kappa_f^2)$ and $l\gg1$,

$$\sum_{l=l_1}^{\infty}\sum_{l_f}\hat{\Omega}_{l_f l}\sim 12(2J_>+1)\pi e^{-\pi\xi}\frac{(\kappa_i^2-\kappa_f^2)}{\kappa_i^2}\left[\frac{\kappa_f}{\kappa_i}\right]\times\left\{\sum_{l=l_1+1}^{\infty}\left[\frac{\kappa_f^2}{\kappa_i^2}\right]^{l}+\left[\frac{\kappa_f^2}{\kappa_i^2}\right]^{l_1}\right\} . \tag{65}$$

The sum is a geometric series of ratio κ_f^2/κ_i^2. After performing this simple operation we obtain

$$\sum_{l=l_1+1}^{\infty}\sum_{l_f}\hat{\Omega}_{l_f l}\sim 12(2J_>+1)\pi e^{-\pi\xi}\left[\frac{\kappa_f}{\kappa_i}\right]^{2l_1+1} . \tag{66}$$

If $\xi/\eta_i\ll1$ then $\kappa_f/\kappa_i=(1+\xi/\eta_i)^{-1}\approx1-\xi/\eta_i\approx1$ and we have

$$\sum_{l=l_1+1}^{\infty}\sum_{l_f}\hat{\Omega}_{l_f l}\sim 12(2J_>+1)\pi e^{-\pi\xi}\left[\frac{\kappa_f}{\kappa_i}\right]^{2l_1} , \qquad l_1\gg\frac{\kappa_i^2}{\kappa_i^2-\kappa_f^2} . \tag{67}$$

2. JWKB approximation

In this approximation the integrals I_0 are expressed in terms of modified Hankel functions [11,13] and for $\varepsilon\xi\gg1$, $l\gg1$, and $l\gg\eta$ one obtains [18]

$$I_0(\kappa_1 l,\kappa_2 l+1;1)\approx\pi^{1/2}2^{-(2p+1/2)}e^{-(|\xi|/\eta)(l+1)}\frac{|\xi|}{\eta}\times\left[(l+1)\frac{|\xi|}{\eta}\right]^{-(p+1/2)} , \tag{68}$$

where

$$p=\begin{cases}0 & \text{if } \kappa_1<\kappa_2\\ 1 & \text{if } \kappa_1>\kappa_2\end{cases} ,$$

$$\xi=\eta_2-\eta_1,\quad \varepsilon=\frac{\left[\eta^2+\left[l+\frac{\alpha}{2}\right]\left[l+1+\frac{\alpha}{2}\right]\right]^{1/2}}{\eta} , \tag{69}$$

$\alpha=\pm1$, and $\eta=(\eta_1+\eta_2)/2$.

Notice that if $l\gg1$ and $l\gg\eta$ then $\xi\varepsilon\gg1$ implies $\xi l/\eta\gg1$ (or $l\gg2\kappa^2/|\kappa_1^2-\kappa_2^2|$), where $\kappa=(\kappa_1+\kappa_2)/2$ and contributions of order $(\xi/\eta)^2$ are neglected.

Replacing Eqs. (68) and (60) into Eq. (41) we also end up with operations involving geometric series. In this case the ratio of the geometric series is $e^{-2\xi/\eta}$, which allows us to write

$$\sum_{l=l_1+1}^{\infty}\sum_{l_f}\hat{\Omega}_{l_j l}\simeq 12(2J_>+1)\pi e^{-\pi\xi}e^{-(\xi/\eta)2l_1}\frac{(2\xi/\eta)}{(e^{2\xi/\eta}-1)} , \qquad l_1\gg\frac{2\kappa^2}{\kappa_i^2-\kappa_f^2} . \tag{70}$$

If $2\xi/\eta\ll1$, i.e., $E_{if}/E\ll1$, where $E=(E_i+E_f)/2$, we have

$$\sum_{l=l_1+1}^{\infty}\sum_{l_f}\hat{\Omega}_{l_f l}\simeq 12(2J_>+1)\pi e^{-\pi\xi}e^{-(\xi/\eta)2l_1} , \qquad l_1\gg\frac{2\kappa^2}{|\kappa_i^2-\kappa_f^2|} . \tag{71}$$

Equation (71) is equivalent to Eq. (67) to first order in (ξ/η).

V. THE NONRELATIVISTIC HIGH-ENERGY LIMIT $E_i\to\infty$

The Born approximation for the scaled collision strength $\hat{\Omega}_{if}$, in the particular case of one electron outside closed shells, is given by

$$\hat{\Omega}_{if}^{B}=(Z_1+1)^2\sum_{\lambda\,(\geq1)}C_\lambda(J_i,J_f)\int_{q_{\min}}^{q_{\max}}\left[\int_0^\infty\mathcal{P}(n_iL_i|u)\mathcal{P}(n_fL_f|u)\,j_\lambda\left[\frac{qu}{(Z_1+1)}\right]du\right]^2 q^{-3}dq , \tag{72}$$

where $q_{\min}=k_i-k_f$, $q_{\max}=k_i+k_f$, j_λ is the spherical Bessel function of order λ, and

$$C_\lambda(J_i,J_f)=8(2\lambda+1)(2L_i+1)(2L_f+1)(2J_i+1)\times(2J_f+1)\begin{bmatrix}\lambda & L_i & L_f\\ 0 & 0 & 0\end{bmatrix}^2\begin{Bmatrix}L_i & J_i & \frac{1}{2}\\ J_f & L_f & \lambda\end{Bmatrix}^2 . \tag{73}$$

For dipole-allowed transitions, the collision strength reduces to

$$\hat{\Omega}_{if}^{B}=\frac{8\omega_i}{E_{if}}\int_{q_{\min}}^{q_{\max}}\frac{\hat{f}(q)}{q}dq , \tag{74}$$

where

$$\hat{f}(q)=\frac{C_1}{8}E_{if}\frac{(Z_1+1)^2}{\omega_i q^2}\times\left[\int_0^\infty \mathcal{P}(n_iL_i|u)\mathcal{P}(n_fL_f|u)j_1\left[\frac{qu}{(Z_1+1)}\right]du\right]^2 . \tag{75}$$

Burgess and Tully [21] have shown that the high-energy limiting behavior of $\hat{\Omega}^B_{if}$, deduced from the Bethe approximation, is given by

$$\hat{\Omega}^B_{if}\underset{E_i\to\infty}{\sim}\frac{4\omega_i\hat{f}}{E_{if}}\ln\left[\frac{4E_i}{E_{if}}\right] , \tag{76}$$

and upon making the substitutions $C_1=8(2J_>+1)$ and $\int_0^\infty \mathcal{P}_{2s}\mathcal{P}_{2p}j_1[qu/(Z_1+1)]du=-q\sqrt{3}/(Z_1+1)$ we obtain the expression

$$\hat{\Omega}^B_{if}\sim 12(2J_>+1)\ln\left[\frac{4E_i}{E_{if}}\right] , \tag{77}$$

where $J_>=\max(J_i,J_f)$ and E_{if} is the transition energy.

For the quadrupole transition $2p_{1/2}$-$2p_{3/2}$, we perform the integration in Eq. (72), with $C_2=32$, $q_{\min}=0$, $q_{\max}=\infty$, $\mathcal{P}_{2p}(u)=24^{-1/2}u^2e^{-u/2}$, and $j_2(t)=(3/t^3-1/t)\sin t-(3/t^2)\cos t$, and we obtain the result

$$\hat{\Omega}^B_{if}(2p_{1/2}\text{-}2p_{3/2})=\tfrac{64}{7} . \tag{78}$$

VI. INTERPOLATION OF DATA

We interpolate the data, using the interactive graphics computer program OMEUPS. Burgess and Tully [22] have developed this new method to assess and compact collision strength data for electron-impact excitation of positive ions. The procedure has not been previously used for proton-impact excitation of positive ions. The originality of the method hinges on the use of scaling techniques which (i) remove the main energy dependence from the data and (ii) map the entire range of E onto the interval [0,1]. We denote the reduced variables by $E_{\rm red},\Omega_{\rm red}$. For optically allowed transitions

$$E_{\rm red}=1-\frac{\ln C}{\ln\left[\frac{E_f}{E_{if}}+C\right]} \tag{79}$$

and

$$\Omega_{\rm red}=\frac{\hat{\Omega}}{\ln\left[\frac{E_f}{E_{if}}+e\right]} , \tag{80}$$

where $C>1$, $e=2.718\ldots$, and

$$\Omega_{\rm red}(0)=\hat{\Omega}(0) , \tag{81}$$

and for the transitions $2p_{1/2}$-$2s_{1/2}$ and $2s_{1/2}$-$2p_{3/2}$

$$\Omega_{\rm red}(1)=12(2J_>+1) . \tag{82}$$

For an optically forbidden transition,

$$E_{\rm red}=\frac{E_f/E_{if}}{(E_f/E_{if}+C)} \tag{83}$$

and

$$\Omega_{\rm red}=\hat{\Omega} , \tag{84}$$

where

$$\Omega_{\rm red}(0)=\hat{\Omega}(0) , \tag{85}$$

and for the transition $2p_{1/2}$-$2p_{3/2}$

$$\Omega_{\rm red}(1)=\hat{\Omega}^{\rm Born}=\tfrac{64}{7} . \tag{86}$$

The parameter C depends on the transition; its value can be adjusted in order to optimize the plot of $\Omega_{\rm red}$ prior to making a spline fit. This fitting procedure has been designed for electron-impact excitation of ionized species, for which $\hat{\Omega}(0)\neq 0$, but $\hat{\Omega}(0)=0$ for proton-impact excitation. The application of the method to proton-impact excitation may give poor accuracy near the excitation threshold. We are concerned, however, with the higher-energy data points which have deviations from the fit less than 1%. After inputting the data in the OMEGA branch and providing an initial estimate for C, the collision strength is scaled and displayed as a function of $E_{\rm red}$. By modifying the value of C one can change the distribution of data points on the plot. We positioned the data so that we got a reasonable fit (rms error less than 1%) for higher energies and we also determined the lower limit of validity of our fit. The program then uses a five-point least-squares spline to fit the scaled data and draws the corresponding curve on the screen. The spline function $y_s(x)$ for $\Omega_{\rm red}$ is tabulated at the five equidistant reduced energy knots $x\equiv E_{\rm red}=0.0,0.25,0.5,0.75,1.0$. The knots specify completely the cubic spline over the given interval. The original data can in this way be readily interpolated or extrapolated. The spline function $y_s(x)$, which allows one to interpolate $y(x)\equiv\Omega_{\rm red}$, using the values $y_s(0)$, $y_s(0.25)$, $y_s(0.75)$, $y_s(1)$, and C, is given in Appendix C of Ref. [22] in the convenient form of a short computer program. The advantage of using this fitting technique is that it allows an extrapolation beyond the range in which the original data are calculated based on the constraint of a correct asymptotic energy behavior. Other fitting techniques have often been based on simple global analytic expression of the type

$$\hat{\Omega}=\sum_{N=0}^{N_{\max}}C_N\left[\frac{E_f}{E_{if}}\right]^{-N}+D\ln\left[\frac{E_i}{E_{if}}\right] , \tag{87}$$

with the parameters C_N and D determined by a method of least squares. These fitting techniques are not appropriate for extrapolation in the case of electric dipole allowed transitions since they do not give an adequate constrain on the logarithmic term which is the leading term at high energies.

VII. RESULTS

We give in Table I the transition energies E_{if} (Ry) between the $n=2$ states of hydrogenlike ions and the re-

TABLE I. Hydrogenlike ions energy splittings among the $n=2$ and reduced mass M of proton and ion in electron-mass units.

Ion	E_{if} (Ry) $2p_{1/2}$-$2s_{1/2}$	$2s_{1/2}$-$2p_{3/2}$	$2p_{1/2}$-$2p_{3/2}$	M
He^+	4.27×10^{-6}	4.898×10^{-5}	5.325×10^{-5}	1466.9
C^{5+}	2.38×10^{-4}	4.082×10^{-3}	4.32×10^{-3}	1694.0
Mg^{11+}	2.84×10^{-3}	6.676×10^{-2}	6.96×10^{-2}	1762.1
S^{15+}	7.87×10^{-3}	2.126×10^{-1}	2.2044×10^{-1}	1780.1
Ar^{17+}	1.2×10^{-2}	3.42×10^{-1}	3.54×10^{-1}	1791.0

duced mass M of proton and ion in electron mass units [23]. In Tables II and III we present a sample of the collision parameters ξ, ξ/η_i, $\xi l_1/\eta_i$, η_i/l_1, and $x=E_{if}/E_i$ for the dipole transitions $2p_{1/2}$-$2s_{1/2}$ in He^+ and $2s_{1/2}$-$2p_{3/2}$ in Ar^{17+}, respectively. The total scaled collision strengths $\hat{\Omega}_{if}$ are given in Tables IV–IX for proton-impact excitation of the dipole $2p_{1/2}$-$2s_{1/2}$ and $2s_{1/2}$-$2p_{3/2}$ transitions and the quadrupole $2p_{1/2}$-$2p_{3/2}$ transition in He^+, C^{5+}, Mg^{11+}, S^{15+}, Ar^{17+}, and $Z_1=\infty$. In the limiting case $Z_1=\infty$ we have used the same transitions energies as in Ar^{17+}. We present in the same tables J_0, the value of total angular momentum at which the short-range interaction becomes negligible, and the value l_1 of the proton orbital angular momentum at which the approximations discussed in Sec. IV A become valid, namely $\hat{\mathbf{T}}^{\mathrm{CBeII}}\sim\hat{\mathbf{T}}^{\mathrm{CBeI}}=-2i\hat{\mathbf{R}}^{\mathrm{CBe}}$ within 1% error. We observe that, for a particular ion, J_0 increases as K_i^2 increases and, for K_i^2 fixed, J_0 increases with the nuclear charge. This is expected since $E_i=M(Z_1+1)^2Z_2^2K_i^2$ (Ry) and for larger impact energies, the incident proton penetrates further into the electron cloud of the ion. As a result, a larger angular momentum J_0 is needed to prevent close encounters. We also notice that l_1 decreases as the nuclear charge increases. Since l_1 is the value at which the I approximation (weak coupling) to the $\hat{\mathbf{T}}$ matrix is valid, it measures the strength of the coupling in the channels. Therefore as the nuclear charge increases, the coupling between channels decreases. In the limiting case $Z_1=\infty$, $\hat{\mathbf{T}}^{\mathrm{CBeII}}=\hat{\mathbf{T}}^{\mathrm{CBeI}}$ and $l_1=J_0-\frac{1}{2}$. We also present the high-angular-momentum contribution $\hat{\Omega}^{\infty}_{l_1+1}=\sum_{l_i=l_1+1}^{\infty}\sum_{l_f}\hat{\Omega}_{l_fl_i}$, calculated using Eq. (51). For the dipole-allowed transition $2p_{1/2}$-$2s_{1/2}$ the contribution $\hat{\Omega}^{\infty}_{l_1+1}$ ranges approximately, for all the ions, from 60% of the total $\hat{\Omega}_{if}$ at $K_i^2=8.0\times10^{-4}$ to 77% at $K_i^2=1.7\times10^{-2}$. For the transition $2s_{1/2}$-$2p_{3/2}$, the contribution $\hat{\Omega}^{\infty}_{l_1+1}$ varies more strongly as a function of K_i^2, owing to the larger transition energy E_{if}. For He^+, it varies from 46% at the lowest value of the parameter K_i to 69% at the largest value of the parameter K_i, and for Ar^{17+} it varies from 1% to 61%.

In Figs. 1–3 we present examples of the reduced data for He^+, Mg^{11+}, and Ar^{17+}. Table X contains the spline fit parameters for He^+, C^{5+}, Mg^{11+}, S^{15+}, and Ar^{17+}.

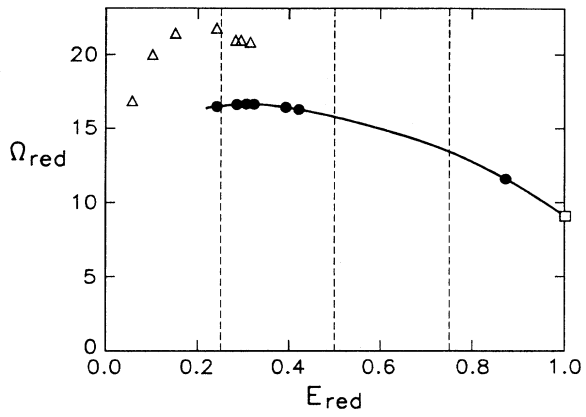

FIG. 2. Reduced collision strength Ω_{red} for the $2p_{1/2}$-$2p_{3/2}$ transition in Mg^{11+}, plotted against reduced energy E_{red}. ●, reduced data; ——, spline fit to the reduced data; △, close coupling (Ref. [10]); □, Born limit.

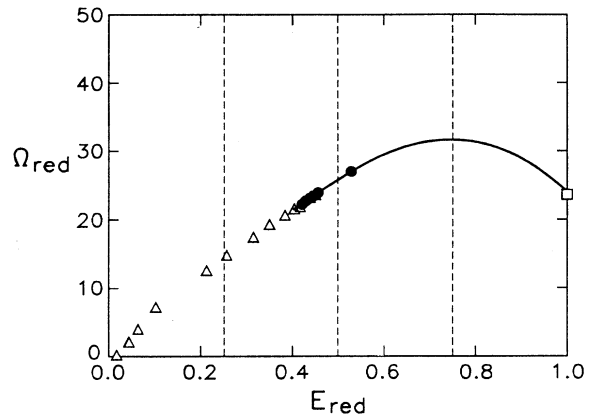

FIG. 1. Reduced collision strength Ω_{red} for the $2p_{1/2}$-$2s_{1/2}$ transition in He^+, plotted against reduced energy E_{red}. ●, reduced data; ——, spline fit to the reduced data; Δ, close coupling (Ref. [10]); □, Born limit.

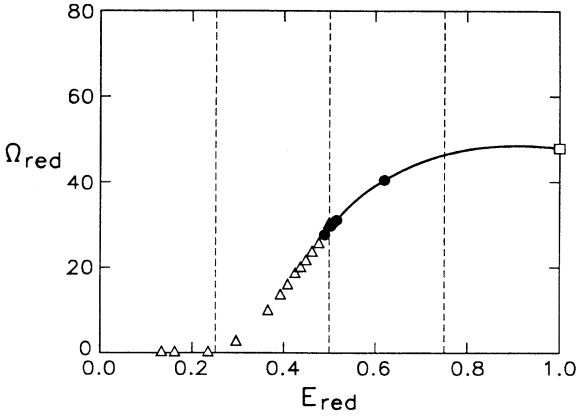

FIG. 3. Reduced collision strength Ω_{red} for the $2s_{1/2}$-$2p_{3/2}$ transition in Ar^{17+}, plotted against reduced energy E_{red}. ●, reduced data; ——, spline fit to the reduced data; △, close coupling (Ref. [10]); □, Born limit.

TABLE II. Collision parameters for the dipole-allowed transition $2p_{1/2}$-$2s_{1/2}$ in He^+. The parameters are defined by Eqs. (22)–(24) and $l_1 = 32\,837$. K_i is numerically equal to the magnitude of the initial scaled velocity of relative motion $v_i/(Z_1+1)Z_2$ in Hartree's atomic units ($2.187\,69\times10^8$ cm s^{-1}).

K_i^2	ξ	ξ/η_i	$\xi l_1/\eta_i$	η_i/l_i	η_i	$x=E_{if}/E_i$
8.0×10^{-4}	8.04×10^{-6}	4.55×10^{-7}	1.49×10^{-2}	5.38×10^{-4}	17.68	9.1×10^{-7}
1.0×10^{-3}	5.75×10^{-6}	3.64×10^{-7}	1.19×10^{-2}	4.81×10^{-4}	15.81	7.3×10^{-7}
1.2×10^{-3}	4.38×10^{-6}	3.03×10^{-7}	9.96×10^{-3}	4.40×10^{-4}	14.43	6.1×10^{-7}
1.4×10^{-3}	3.41×10^{-6}	2.60×10^{-7}	8.53×10^{-3}	4.07×10^{-4}	13.36	5.2×10^{-7}
1.6×10^{-3}	2.84×10^{-6}	2.27×10^{-7}	7.47×10^{-3}	3.81×10^{-4}	12.50	4.5×10^{-7}
1.8×10^{-3}	2.38×10^{-6}	2.02×10^{-7}	6.64×10^{-3}	3.59×10^{-4}	11.78	4.0×10^{-7}
1.7×10^{-2}	8.21×10^{-8}	2.14×10^{-8}	7.03×10^{-4}	1.17×10^{-4}	3.83	4.3×10^{-8}

TABLE III. Collision parameters for the dipole-allowed transition $2s_{1/2}$-$2p_{3/2}$ in Ar^{17+}. The parameters are defined by Eqs. (22)–(24) and $l_1 = 4455$. K_i is numerically equal to the magnitude of the initial scaled velocity of relative motion $v_i/(Z_1+1)Z_2$ in Hartree's atomic units ($2.187\,69\times10^8$ cm s^{-1}).

K_i^2	ξ	ξ/η_i	$\xi l_1/\eta_i$	η_i/l_i	η_i	$x=E_{if}/E_i$
8.0×10^{-4}	1.23×10^{-2}	3.68×10^{-4}	1.64	7.49×10^{-3}	33.4	7.4×10^{-4}
1.0×10^{-3}	8.8×10^{-3}	2.95×10^{-4}	1.31	6.70×10^{-3}	29.9	5.9×10^{-4}
1.2×10^{-3}	6.7×10^{-3}	2.46×10^{-4}	1.10	6.12×10^{-3}	27.3	4.9×10^{-4}
1.4×10^{-3}	5.31×10^{-3}	2.1×10^{-4}	0.93	5.67×10^{-3}	25.2	4.2×10^{-4}
1.6×10^{-3}	4.35×10^{-3}	1.84×10^{-4}	0.82	5.30×10^{-3}	23.6	3.7×10^{-4}
1.8×10^{-3}	3.64×10^{-3}	1.64×10^{-4}	0.73	5.0×10^{-3}	22.3	3.3×10^{-4}
1.7×10^{-2}	1.25×10^{-4}	1.73×10^{-5}	7.7×10^{-2}	1.62×10^{-3}	7.2	3.5×10^{-5}

TABLE IV. Total scaled collision strength $\hat{\Omega}$ and high-angular-momentum contribution $\hat{\Omega}_{l_1+1}^{\infty}$ for proton-impact excitation of He^+. Short-range contribution becomes negligible for $J > J_0$. K_i is numerically equal to the magnitude of the initial scaled velocity of relative motion $v_i/(Z_1+1)Z_2$ in Hartree's atomic units ($2.187\,69\times10^8$ cm s^{-1}).

			$2p_{1/2}$-$2s_{1/2}$		$2p_{1/2}$-$2p_{3/2}$		$2s_{1/2}$-$2p_{3/2}$	
K_i^2	J_0	l_1	$\hat{\Omega}_{l_1+1}^{\infty}$	$\hat{\Omega}$	$\hat{\Omega}_{l_1+1}^{\infty}$	$\hat{\Omega}$	$\hat{\Omega}_{l_1+1}^{\infty}$	$\hat{\Omega}$
8.0×10^{-4}	526.5	32 837	207.3	313.3	0.049	15.95	180.5	392.4
1.0×10^{-3}	590.5	32 837	218.1	324.1	0.048	15.95	201.9	413.8
1.2×10^{-3}	648.5	32 837	226.8	332.7	0.047	15.96	219.4	431.3
1.4×10^{-3}	701.5	32 837	234.2	340.1	0.046	15.97	234.2	446.1
1.6×10^{-3}	749.5	32 837	240.6	346.6	0.044	15.98	247.0	458.9
1.8×10^{-3}	794.5	32 837	246.8	352.8	0.043	15.98	258.3	470.3
1.7×10^{-2}	2499.5	32 838	354.1	460.6	0.011	16.40	473.9	686.6

TABLE V. Total scaled collision strength $\hat{\Omega}$ and high-angular-momentum contribution $\hat{\Omega}_{l_1+1}^{\infty}$ for proton-impact excitation of C^{5+}. Short-range contribution becomes negligible for $J > J_0$. K_i is numerically equal to the magnitude of the initial scaled velocity of relative motion $v_i/(Z_1+1)Z_2$ in Hartree's atomic units ($2.187\,69\times10^8$ cm s^{-1}).

			$2p_{1/2}$-$2s_{1/2}$		$2p_{1/2}$-$2p_{3/2}$		$2s_{1/2}$-$2p_{3/2}$	
K_i^2	J_0	l_1	$\hat{\Omega}_{l_1+1}^{\infty}$	$\hat{\Omega}$	$\hat{\Omega}_{l_1+1}^{\infty}$	$\hat{\Omega}$	$\hat{\Omega}_{l_1+1}^{\infty}$	$\hat{\Omega}$
8.0×10^{-4}	573.5	12 640	172.6	278.6	0.069	16.08	72.3	284.2
1.0×10^{-3}	666.5	12 640	178.2	289.4	0.057	16.17	93.7	305.7
1.2×10^{-3}	749.5	12 640	192.0	298.1	0.047	16.24	111.2	323.2
1.4×10^{-3}	824.5	12 640	199.4	305.6	0.040	16.31	126.0	338.1
1.6×10^{-3}	894.5	12 640	205.8	312.1	0.034	16.37	138.8	351.1
1.8×10^{-3}	958.5	12 640	211.5	317.9	0.030	16.41	150.1	362.5
1.7×10^{-2}	2499.5	12 644	319.2	424.6	0.003	14.3	365.7	575.0

TABLE VI. Total scaled collision strength $\hat{\Omega}$ and high-angular-momentum contribution $\hat{\Omega}_{l_1+1}^{\infty}$ for proton-impact excitation of Mg^{11+}. Short-range contribution becomes negligible for $J > J_0$. K_i is numerically equal to the magnitude of the initial scaled velocity of relative motion $v_i/(Z_1+1)Z_2$ in Hartree's atomic units ($2.187\,69\times10^8$ cm s^{-1}).

			$2p_{1/2}$-$2s_{1/2}$		$2p_{1/2}$-$2p_{3/2}$		$2s_{1/2}$-$2p_{3/2}$	
K_i^2	J_0	l_1	$\hat{\Omega}_{l_1+1}^{\infty}$	$\hat{\Omega}$	$\hat{\Omega}_{l_1+1}^{\infty}$	$\hat{\Omega}$	$\hat{\Omega}_{l_1+1}^{\infty}$	$\hat{\Omega}$
8.0×10^{-4}	676.5	6574	153.4	259.8	0.028	16.49	3.6	216.0
1.0×10^{-3}	774.5	6574	164.1	270.7	0.019	16.59	25.0	237.7
1.2×10^{-3}	862.5	6574	172.8	279.6	0.014	16.60	42.5	255.4
1.4×10^{-3}	943.5	6574	180.2	287.1	0.011	16.54	57.3	270.4
1.6×10^{-3}	1018.5	6575	186.6	293.6	0.009	16.44	70.1	283.4
1.8×10^{-3}	1089.5	6575	192.3	299.4	0.007	16.31	81.5	294.8
1.7×10^{-2}	2499.5	6582	300.0	394.4	0.001	11.6	297.0	483.5

TABLE VII. Total scaled collision strength $\hat{\Omega}$ and high-angular-momentum contribution $\hat{\Omega}_{l_1+1}^{\infty}$ for proton-impact excitation of S^{15+}. Short-range contribution becomes negligible for $J > J_0$. K_i is numerically equal to the magnitude of the initial scaled velocity of relative motion $v_i/(Z_1+1)Z_2$ in Hartree's atomic units ($2.187\,69\times10^8$ cm s^{-1}).

			$2p_{1/2}$-$2s_{1/2}$		$2p_{1/2}$-$2p_{3/2}$		$2s_{1/2}$-$2p_{3/2}$	
K_i^2	J_0	l_1	$\hat{\Omega}_{l_1+1}^{\infty}$	$\hat{\Omega}$	$\hat{\Omega}_{l_1+1}^{\infty}$	$\hat{\Omega}$	$\hat{\Omega}_{l_1+1}^{\infty}$	$\hat{\Omega}$
8.0×10^{-4}	705.5	4981	145.9	252.5	0.015	16.62		
1.0×10^{-3}	805.5	4981	156.6	263.4	0.01	16.56		
1.2×10^{-3}	895.5	4981	165.3	272.3	0.007	16.38	14.2	227.2
1.4×10^{-3}	978.5	4981	172.7	279.6	0.006	16.14	29.0	241.8
1.6×10^{-3}	1055.5	4982	179.1	285.9	0.005	15.88	41.8	254.3
1.8×10^{-3}	1127.5	4982	184.8	291.4	0.004	15.62	53.1	265.2
1.7×10^{-2}	2499.5	4991	292.5	379.7	0.001	10.8	268.5	439.7

TABLE VIII. Total scaled collision strength $\hat{\Omega}$ and high-angular-momentum contribution $\hat{\Omega}_{l_1+1}^{\infty}$ for proton-impact excitation of Ar^{17+}. Short-range contribution becomes negligible for $J > J_0$. K_i is numerically equal to the magnitude of the initial scaled velocity of relative motion $v_i/(Z_1+1)Z_2$ in Hartree's atomic units ($2.187\,69\times10^8$ cm s^{-1}).

			$2p_{1/2}$-$2s_{1/2}$		$2p_{1/2}$-$2p_{3/2}$		$2s_{1/2}$-$2p_{3/2}$	
K_i^2	J_0	l_1	$\hat{\Omega}_{l_1+1}^{\infty}$	$\hat{\Omega}$	$\hat{\Omega}_{l_1+1}^{\infty}$	$\hat{\Omega}$	$\hat{\Omega}_{l_1+1}^{\infty}$	$\hat{\Omega}$
8.0×10^{-4}	717.5	4455	142.6	249.3	0.011	16.60		
1.0×10^{-3}	819.5	4455	153.3	260.2	0.008	16.44		
1.2×10^{-3}	910.5	4455	162.0	268.8	0.006	16.16	2.4	215
1.4×10^{-3}	993.5	4455	169.4	276.1	0.004	15.84	17.3	229.5
1.6×10^{-3}	1071.5	4455	175.8	282.2	0.003	15.52	30.1	241.6
1.8×10^{-3}	1144.4	4455	181.5	287.7	0.003	15.21	41.4	252.3
1.7×10^{-2}	2499.5	4466	289.2	373.0	0.001	10.5	256.7	420.8

TABLE IX. Total scaled collision strength $\hat{\Omega}$ and high-angular-momentum contribution $\hat{\Omega}^{\infty}_{l_1+1}$ for proton-impact excitation of $Z_1=\infty$. Transition energies E_{if} correspond to Ar^{17+}. Short-range contribution becomes negligible for $J>J_0$. K_i is numerically equal to the magnitude of the initial scaled velocity of relative motion $v_i/(Z_1+1)Z_2$ in Hartree's atomic units ($2.187\,69\times10^8$ cm s^{-1}).

			$2p_{1/2}$-$2s_{1/2}$		$2p_{1/2}$-$2p_{3/2}$		$2s_{1/2}$-$2p_{3/2}$	
K_i^2	J_0	l_1	$\hat{\Omega}^{\infty}_{l_1+1}$	$\hat{\Omega}$	$\hat{\Omega}^{\infty}_{l_1+1}$	$\hat{\Omega}$	$\hat{\Omega}^{\infty}_{l_1+1}$	$\hat{\Omega}$
8.0×10^{-4}	805.5	805	224.6	319.2	0.74	8.37	127.6	316.9
1.0×10^{-3}	908.5	908	229.6	324.9	0.74	8.27	137.5	328.2
1.2×10^{-3}	1000.5	1000	233.7	329.6	0.74	8.27	145.8	337.6
1.4×10^{-3}	1085.5	1085	237.2	333.6	0.74	8.31	152.8	345.7
1.6×10^{-3}	1164.5	1164	240.2	337.2	0.74	8.36	158.9	352.8
1.8×10^{-3}	1237.5	1237	244.4	341.8	0.74	8.41	164.3	359.1
1.7×10^{-2}	2499.5	2499	317.0	407.6	1.75	9.08	181.1	493.6

Also shown are the close-coupling (CC) results of Zygelman and Dalgarno [10]. For the dipole transitions in the He^+-Ar^{17+} ions the agreement is excellent. The largest differences are 5% for the transition $2s_{1/2}$-$2p_{3/2}$ in Ar^{17+} at $E_i=480$ Ry and 3% at $E_i=800$ Ry.

In the case of the $2p_{1/2}$-$2p_{3/2}$ transition the discrepancies between their results and ours are larger for ions of low Z_1. The discrepancies range from 35% in He^+ to 9% in Ar^{17+}. This discrepancy is presumably due to close coupling effects included in the calculations of Zygelman and Dalgarno. Zygelman and Dalgarno [24] selected an angular momentum, which they denoted J_{CB}, and used the CC approximation for $\frac{1}{2}\le J\le J_{CB}$ and a unitarized Coulomb-Born (CB) approximation for $J>J_{CB}$. In their CB approximation the integrals $I(\kappa_i l_i,\kappa_f l_f;1)$ and $I(\kappa_i l_i,\kappa_f l_f;2)$ were evaluated using the WKB approximation. Our unitarized CB approximation uses the Coulomb-Born approximation [Eqs. (25)–(27)] to calcu-

TABLE X. Values of the spline function $y_s(x)$ for $\hat{\Omega}_{red}$ at the five reduced energy knots. E_{min} is the lower limit of validity of the spline fit. The parameter C is chosen to minimize the rms error of each fit.

			Spline function					
Transition	E_{min} (Ry)	C	$y_s(0)$	$y_s(\frac{1}{4})$	$y_s(\frac{1}{2})$	$y_s(\frac{3}{4})$	$y_s(1)$	rms error
				He^+				(%)
$2p_{1/2}$-$2s_{1/2}$	4.694	3×10^3	63.09	21.53	25.97	31.74	23.93	0.03
$2s_{1/2}$-$2p_{3/2}$	4.694	3×10^3	3.208	29.22	51.94	68.55	47.87	0.01
$2p_{1/2}$-$2p_{3/2}$	4.694	6×10^5	15.94	15.98	16.41	16.48	9.143	0.01
				C^{5+}				
$2p_{1/2}$-$2s_{1/2}$	48.787	2×10^3	23.55	18.72	27.67	31.64	24.02	0.01
$2s_{1/2}$-$2p_{3/2}$	48.783	3×10^2	2.448	15.57	41.94	59.86	47.90	0.01
$2p_{1/2}$-$2p_{3/2}$	48.783	5×10^4	15.53	16.24	16.63	15.61	9.143	0.01
				Mg^{11+}				
$2p_{1/2}$-$2s_{1/2}$	202.991	5×10^2	119.3	27.55	27.75	28.39	24.01	0.01
$2s_{1/2}$-$2p_{3/2}$	202.924	10^2	91.39	16.65	35.79	50.95	48.07	0.01
$2p_{1/2}$-$2p_{3/2}$	202.924	9×10^3	13.60	16.51	15.86	13.47	9.143	0.02
				S^{15+}				
$2p_{1/2}$-$2s_{1/2}$	364.6	3×10^2	230.9	41.68	24.92	27.80	24.01	0.01
$2s_{1/2}$-$2p_{3/2}$	546.6	80	46.46	10.82	35.32	47.25	47.99	0.01
$2p_{1/2}$-$2p_{3/2}$	364.3	3×10^3	11.57	16.51	15.17	12.43	9.143	0.01
				Ar^{17+}				
$2p_{1/2}$-$2s_{1/2}$	464.215	3×10^2	129.4	28.15	25.29	27.10	24.29	0.02
$2s_{1/2}$-$2p_{3/2}$	695.986	50	486.0	63.47	29.77	46.58	47.99	0.02
$2p_{1/2}$-$2p_{3/2}$	463.873	3×10^3	11.57	16.51	15.17	12.43	9.143	0.01

TABLE XI. Extrapolated total scaled collision strength for proton-impact excitation of fine-structure transitions in He^+ and Ar^{17+}. Scaled collision strength for electron-impact excitation of He^+ and $Z_1=\infty$ (Ref. [11]). K_i is numerically equal to the magnitude of the initial scaled velocity of relative motion $v_i/(Z_1+1)Z_2$ in Hartree's atomic units ($2.187\,69\times10^8$ cm s^{-1}).

	$2p_{1/2}$-$2s_{1/2}$				$2s_{1/2}$-$2p_{3/2}$			
			Electrons Ref. [11]				Electrons Ref. [11]	
K_i^2	He^+	Ar^{17+}	He^+	$Z_1=\infty$	He^+	Ar^{17+}	He^+	$Z_1=\infty$
0.05	509	407	557	584	786	487	880	934
0.15	557	439	586	613	886	553	938	993
0.25	578	453	598	624	931	582	961	1014
0.75	623	482	621	642	1026	643	1009	1050
1.25	643	496	632	649	1069	671	1031	1064
2.25	666	511	646	657	1117	703	1057	1080
3.25	681	520	654	663	1147	722	1074	1092

late $I(\kappa_i l_i,\kappa_f l_f;1)$ and $I(\kappa_i l_i,\kappa_f l_f;2)$ for $\xi\ll1$, $\xi/\eta_i\ll1$, and $l_1\xi/\eta_i\lesssim1$.

We find that the short-range interaction [Eqs. (16) and (17)], describing electron-cloud penetration [25], becomes important for the $2p_{1/2}$-$2p_{3/2}$ quadrupole transition at $K_i^2\sim1.0\times10^{-3}$. If short-range effects are not included, the $2p_{1/2}$-$2p_{3/2}$ scaled collision strength $\hat{\Omega}_{if}$ increases by 30% at $K_i^2=1.4\times10^{-3}$ for S^{15+} and Ar^{17+}. The dipole transitions, dominated, on the other hand, by the long-range coupling, are not too sensitive to the effect of the short-range interaction terms, at the values of the parameter K_i considered in this paper. The largest variation, if short-range effects are not included, is 1.5% for the transition $2s_{1/2}$-$2p_{3/2}$ in He^+ at $K_i^2\sim1.2\times10^{-3}$.

We present in Tables XI and XII, as an example, the extrapolated scaled total collision strength for He^+ and Ar^{17+}. We also include the electron impact excitation results of Burgess, Hummer, and Tully [11] for He^+ and $Z_1=\infty$. The scaled total collision strengths of Burgess, Hummer, and Tully for $Z_1=\infty$ are slightly larger ($\sim3\%$) than the collision strengths for He^+.

TABLE XII. Extrapolated total scaled collision strength for proton-impact excitation of fine-structure transitions $2p_{1/2}$-$2p_{3/2}$ in He^+ and Ar^{17+}. Scaled collision strength for electron impact excitation of He^+ and $Z_1=\infty$ (Ref. [11]). K_i is numerically equal to the magnitude of the initial scaled velocity of relative motion $v_i/(Z_1+1)Z_2$ in Hartree's atomic units ($2.187\,69\times10^8$ cm s^{-1}).

			Electrons Ref. [11]	
K_i^2	He^+	Ar^{17+}	He^+	$Z_1=\infty$
0.05	13.13	9.65	12.50	12.76
0.15	10.73	9.32	11.82	11.93
0.25	10.13	9.25	11.29	11.49
0.75	9.48	9.18	10.21	10.57
1.25	9.35	9.16	9.84	10.17
2.25	9.26	9.15	9.46	9.74
3.25	9.22	9.15	9.35	9.56

VIII. CONCLUSIONS

We have developed a scaling technique that applies to the excitation of positive ions by particles of arbitrary charge and mass. To illustrate our approach we have used a unitarized Coulomb-Born approximation to consider collisions involving high-energy incident protons on hydrogenlike ions. We have carried out the calculations, for the excitation of transitions between fine-structure levels involving the $n=2$ principal quantum number, under the assumption that (see Tables I and II) $\xi\ll1$, $\xi/\eta\ll1$, and $\xi l_1/\eta\lesssim1$. For a nonrelativistic energy $E_i\rightarrow\infty$, we have used the Born approximation to obtain the scaled total collision strength $\hat{\Omega}_{if}$ for dipole and quadrupole transitions and these limiting values confirm the correct high-energy behavior of our data. We show that, for dipole-allowed transitions, the dominant part of the scaled total collision strength $\hat{\Omega}_{if}$ comes from large angular momenta $l\gtrsim2000$. These calculations also confirm the significance of electron-cloud penetration for the quadrupole transition $2p_{1/2}$-$2p_{3/2}$, since the strength of short-range effects increases with the nuclear charge and K_i^2 [$E_i=M(Z_1+1)^2Z_2^2K_i^2$ (Ry)]. For the values of the parameter K_i considered in this paper, the present CB approximation gives results in good agreement with previous close-coupling calculations [10].

We intend to extend the calculations of ion-impact collisional transitions amongst fine-structure levels of hydrogenic ions to alkali-metal-like positive ions and ions of the cosmically abundant elements (Al,Si,S,Ba) and to boronlike and fluorinelike systems and other ions likely to occur as impurities in fusion plasmas.

ACKNOWLEDGMENTS

This work was supported in part by the Natural Sciences and Engineering Research Council of Canada (NSERC). One of us (D.W.S.) gratefully acknowledges support from NSERC. We would like to thank Dr. A. Burgess, Dr. C. T. Whelan, Dr. H. P. Summers, and Dr. J. A. Tully for valuable discussions. We also wish to thank A. Burgess for the use of some of his subroutines.

[1] R. A. Phaneuf, in *Atomic Processes in Electron-Ion and Ion-Ion Collisions,* edited by F. Brouillard (Plenum, New York, 1986).
[2] H. P. Summers, P. Thomas, R. Giannella, M. von Hellerman, and members of Experimental Division II, J. Phys. (Paris) Coll. **1**, C1-191 (1991).
[3] S. O. Kastner, Astron. Astrophys. **54**, 255 (1977).
[4] S. O. Kastner and A. K. Bhatia, Astron. Astrophys. **71**, 211 (1979).
[5] P. Faucher, J. Phys. B **8**, 1886 (1975).
[6] I. C. Percival, in *Atoms in Astrophysics,* edited by P. G. Burke, W. B. Eissner, D. G. Hummer, and I. C. Percival (Plenum, New York, 1983), p. 75.
[7] A. Dalgarno, in *Atoms in Astrophysics* (Ref. [6]), p. 103.
[8] R. H. G. Reid, in Adv. At. Mol. Phys. **25**, 251 (1988).
[9] R. S. Walling and J. C. Weisheit, Phys. Rep. **162**, 1 (1988).
[10] B. Zygelman and A. Dalgarno, Phys. Rev. A **35**, 4085 (1987).
[11] A. Burgess, D. G. Hummer, and J. A. Tully, Philos. Trans. R. Soc. London **266**, 225 (1970).
[12] M. C. Chidichimo and T. S. Davison, Phys. Rev. A **42**, 3830 (1990).
[13] K. Alder, A. Bohr, T. Huus, B. Mottelson, and A. Winther, Rev. Mod. Phys. **28**, 432 (1956).
[14] A. Burgess, J. Phys. B **7**, L364 (1974).
[15] V. M. Burke and M. J. Seaton, J. Phys. B **19**, L527 (1986).
[16] V. M. Burke and M. J. Seaton, Proc. Phys. Soc. **77**, 199 (1961).
[17] D. M. Brink and G. R. Satchler, *Angular Momentum* (Oxford University Press, Oxford, 1968).
[18] *Handbook of Mathematical Functions,* edited by M. Abramowitz and I. A. Stegun (Dover, New York, 1972).
[19] I. P. Grant, Mon. Not. R. Astron. Soc. **118**, 241 (1958).
[20] A. Erdélyi *et al., Higher Transcendental Functions* (McGraw-Hill, New York, 1953), Vol. I, p. 76, Eqs. (10) and (12).
[21] A. Burgess and J. A. Tully, J. Phys. B **11**, 11 4271 (1978).
[22] A. Burgess and J. A. Tully, Astron. Astrophys. **254**, 436 (1992).
[23] G. W. Erickson, J. Phys. Chem. Ref. Data **6**, 831 (1977).
[24] There is a misprint in Table I of Ref. [10]. The entries in the last three rows, corresponding to quadrupole coupling coefficients, have the wrong sign.
[25] M. J. Seaton, Mon. Not. R. Astron. Soc. **127**, 191 (1964).